Optics Communications 428 (2018) 104–109

Contents lists available at ScienceDirect

Optics Communications

journal homepage: www.elsevier.com/locate/optcom

Experimental study on subaperture stitching testing of convex hyperboloid surface

Deyan Zhu [b], Lisong Yan [a,*], Xiaokun Wang [c], Ming Li [d], Donglin Ma [a], Lianying Chao [a]

[a] School of Optical and Electronic Information, Huazhong University of Science and Technology, Wuhan, 430074, China
[b] Laser Fusion Research Center, China Academy of Engineering Physics, Mianyang, Sichuan, 621900, China
[c] Key Laboratory of Optical System Advanced Manufacturing Technology, Changchun Institute of Optics, Fine Mechanics and Physics, Chinese Academy of Sciences, Changchun, 130033, China
[d] Intane optics, Nanjing, 210046, China

ARTICLE INFO

Keywords:
Interferometry
Convex aspheric surfaces
Stitching
Non-null testing

ABSTRACT

We propose a non-null subaperture stitching method to measure the convex aspheric surfaces. In the method, the non-null configuration avoids the introduction of auxiliary optical elements which must be specially designed and customized, and their compensating effects cannot be independently measured. In order to obtain the full aperture result, a non-null stitching algorithm based on ray tracing method and least square method is developed to stitch all phase data together. Both simulation and experimental results justify the proposed method.

1. Introduction

Aspheric optical surface has broad applications for its capability in correcting aberrations, improving image quality and reducing the size and weight of the system [1]. Precise and efficient measurement of aspheric optical surface is necessary. Among different surface characterization techniques, interferometry is playing a more and more important role. In interferometry, null testing using null lens or computer-generated hologram (CGH) is an efficient test configuration for small-aperture optical surfaces [2–7]. However, for testing large-aperture optics, especially convex aspheric surfaces, the null testing to the aspheric surface is hard because it is difficult and time consuming to manufacture required large aperture auxiliary elements such as null lens or computer-generated hologram. Instead, the sub-aperture stitching (SAS) testing and the non-null testing can be combined to accomplish the interferometry of the convex aspheric surfaces.

SAS testing has been developed to overcome the aperture size limitations of interferometers. It can obtain the full aperture map without testing the whole mirror at one time, thus it is widely used in measuring large flat mirrors, large convex surfaces and aspheric surfaces exceeding the vertical range of the interferometer. The SAS testing method was first proposed by Kim in 1982, and significantly expanded the dynamic range of an interferometer [8]. According to the testing region shape of the subaperture, there are two major stitching methods: one is the annular stitching method which is widely used in the stitching testing for concave rotational symmetric aspheric surfaces [9–12], and the other one is the circular stitching method which has better generality and expandability [13,14].

In this paper, we propose a simple, efficient non-null stitching technique with circular subapertures to test convex aspheric surfaces. With the proposed method, we characterized a ϕ 260 mm convex hyperboloid surface. The stitching accuracy can be evaluated by the simulation and the experimental results. The paper is organized as follows. In Section 2, the basic theory of the stitching technique involving the retrace error calculation and the stitching algorithm is introduced. In Section 3, the effectiveness of our method is shown in simulation. In Section 4, we demonstrate the technique by testing a ϕ 260 mm convex hyperboloid surface. Finally, the conclusion is given in Section 5.

2. Theory

2.1. The principle of the retrace error correction

The retrace error in the non-null testing can be calculated with ray tracing method. Unlike the null testing, the testing rays in the non-null testing follow different paths from the reference rays. The resulting extra aberration between the measured and the real surface maps is the retrace error. The retrace error should be corrected before stitching as it is not manufactory surface error but an artificial extra aberration due to the non-null testing.

* Corresponding author.
E-mail address: yanlisong@hust.edu.cn (L. Yan).

https://doi.org/10.1016/j.optcom.2018.07.045
Received 6 June 2018; Received in revised form 10 July 2018; Accepted 14 July 2018
Available online 23 July 2018

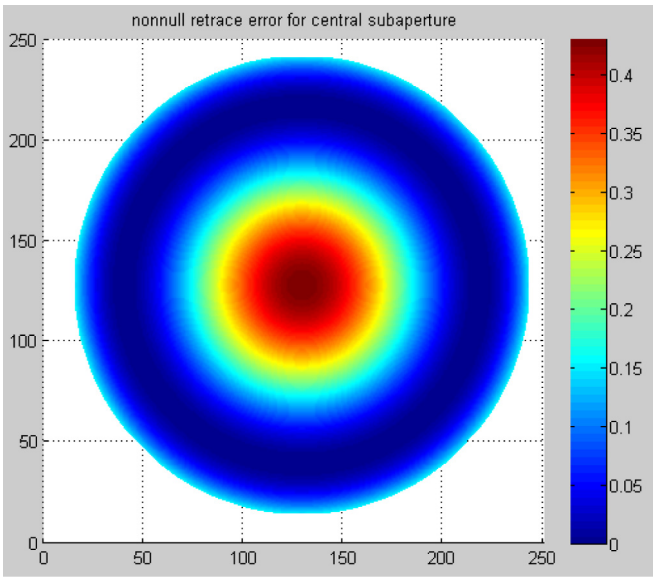

Fig. 1. Retrace error for rotational symmetric subapertures.

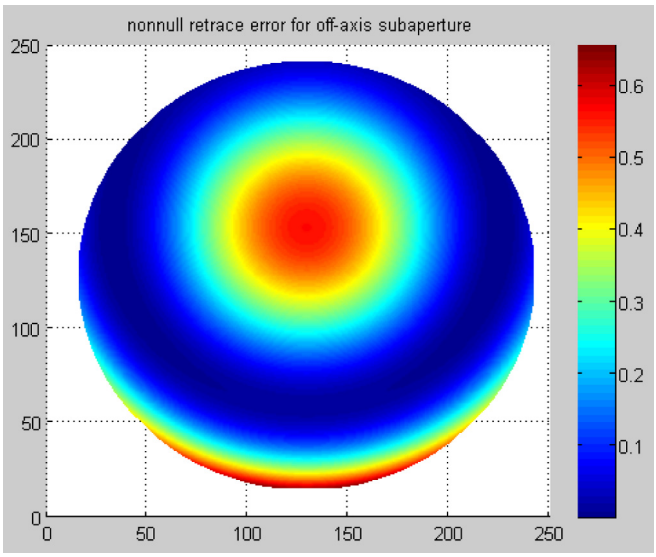

Fig. 2. Retrace error for off-axis subapertures.

The wavefront tested by the interferometer includes both the surface error of the testing aspheric surface and artifacts such as the retrace error, the alignment error, and the retrace coordinate error [15,16]. So the wavefront obtained from the interferometer can be expressed as:

$$W_{interferometer} = W_{retrace} \oplus W_{alignment} \oplus W_{coordinate} \oplus W_{test} \tag{1}$$

where $W_{interferometer}$ is the measured wavefront from the interferometer, $W_{retrace}$ is the retrace error, $W_{alignment}$ is the alignment error between interferometer and the testing aspheric surface and W_{test} is the surface error of the testing aspheric surface. Note that "$\oplus$" in Eq. (1) denotes the variables not simply added up. Thus, the total interferometer error $W_{interferometer}$ depends on all of the retrace error, the alignment error, the retrace coordinate error and the surface error of the aspheric surface.

Assuming an aspheric mirror to be characterized has a subaperture aperture of D_{sub} and a vertex radius of R, the F number of the standard lens should be:

$$F \geq \frac{R}{D_{sub}} \tag{2}$$

According to the designed optical testing path, the retrace error can be calculated in the optical simulation tools such as Zemax or Code V with ray tracing method.

For rotational symmetric subapertures, the retrace error behaves like a combination of power and spherical aberrations as shown in Fig. 1. For the off-axis subapertures, the behavior of the retrace error is shown in Fig. 2.

After calculating the retrace error of each subaperture with the ray tracing method, the retrace error and the retrace coordinate error can be removed from the subaperture testing map at the same time [15,16]. The alignment error of each subaperture will be separated with the stitching algorithm introduced in Section 2.2.

2.2. Stitching algorithm

In order to obtain a full aperture map, a stitching algorithm is developed to stitch each subaperture map together to a whole map.

Currently there are several types of stitching algorithms such as maximum likelihood estimation method, the least square method, and the iteration method. The maximum likelihood estimation method is mainly used in flat mirror stitching, and can calculate the test map and the reference map simultaneously [17]. In the least square method, the full aperture map is reconstructed by compensating the alignment error of each subaperture [18,19]. The iteration method is based on the three-dimensional coordinate transformation [20,21].

Different from the above methods, we propose an algorithm combining the iteration calculation and the least square method.

Our proposed stitching algorithm shown in Fig. 3 is based on the least square method [18,19]. First according to the subaperture arrangement, each subaperture is tested with interferometer and non-null errors are calculated according to the parameters of the vertex radius and the aperture of each subaperture. With the method introduced in Section 2.1, non-null errors can be removed from each subaperture testing result and all the coordinates of each subaperture can be unified in a global coordinate at this time. Then stitching coefficients of each subaperture except the standard one can be calculated with the stitching algorithm discussed in Section 2.2. To improve the stitching accuracy, the residual map of every two adjacent maps is calculated after stitching. If the RMS of the residual map satisfies the criteria, stitching is accomplished. If not, two-dimensional cross-correlation between every two adjacent subapertures is calculated to get a more accurate positioning of each subaperture and the stitching coefficients of each subaperture will be recalculated until the residual meets the requirement.

Assuming there are N subapertures in the measurement. We take the Nth subaperture as a reference, then the ith subaperture can be expressed as:

$$\Phi_i'(x,y) = \Phi_i(x,y) + \sum_{k=1}^{L} a_{ik} f_k(x,y) \tag{3}$$

where $\Phi_i(x,y)$ is the ith subaperture testing map, $f_k(x,y)$ can be any predefined functions, a_{ik} is the stitching coefficient and L is the term number to be fitted. In the non-null stitching, the term number to be fitted between subapertures is nine and the function $f_k(x,y)$ can be written as:

$$\begin{cases} f_1(x,y) = x \\ f_2(x,y) = y \\ f_3(x,y) = x^2 + y^2 \\ f_4(x,y) = xy \\ f_5(x,y) = x^2 - y^2 \\ f_6(x,y) = x(x^2 + y^2) \\ f_7(x,y) = y(x^2 + y^2) \\ f_8(x,y) = (x^2 + y^2)^2 \\ f_9(x,y) = 1 \end{cases} \tag{4}$$

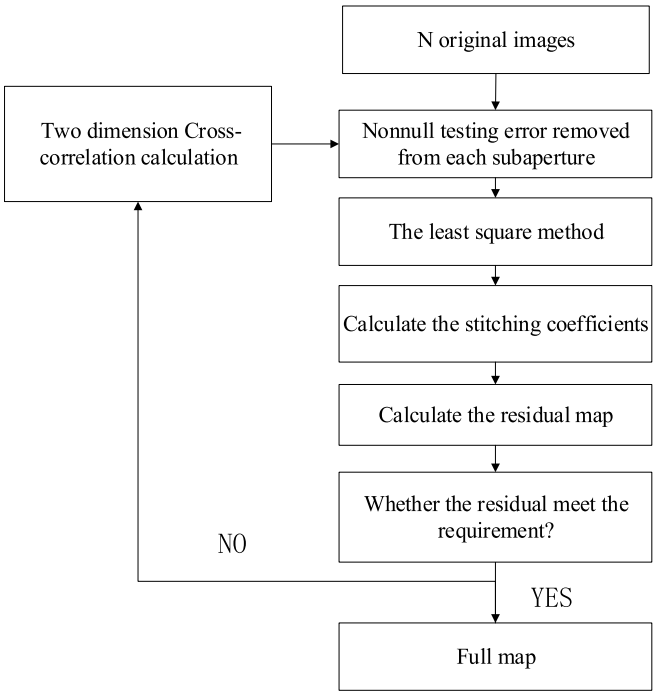

Fig. 3. Flow chart of stitching algorithm.

Then least squared method is applied:

$$\min = \sum_{i=1\ldots N} \sum_{\substack{j=1,\ldots,N \\ j\neq i}}^{i\cap j} [(\Phi_i(x,y) + \sum_{k=1}^{L} a_{ik} f_k(x,y)) - (\Phi_j(x,y) + \sum_{k=1}^{L} a_{jk} f_k(x,y))]^2 \quad (5)$$

For Eq. (5), it can be transformed to a group of linear equation:

$$P = Q \cdot R \quad (6)$$

where P, Q and R are defined as follows:

1. P is a vector in length of $(N-1)\times L$ row. For the $((j-1)\cdot L+k)$th row of the vector element, it can be expressed as:

$$P_{(j-1)\cdot k} = \sum_{\substack{i=1 \\ i\neq j}}^{N} \sum_{i\cap j} f_k(x,y)(\Phi_j(x,y) - \Phi_i(x,y)) \quad (7)$$

2. Q is a matrix in size of $(N-1)\times L$. For the element in the row $((j-1)\cdot L+k)$, column $((l-1)\cdot L+k')$ of the matrix, it can be expressed as:

$$Q_{((j-1)\cdot k)((l-1)\cdot k')} = \begin{cases} -\sum_{\substack{i=1 \\ i\neq j}}^{N} \sum_{i\cap j} f_j(x,y)\cdot f_k(x,y) & j = l \\ \sum_{j\cap l} f_j(x,y)\cdot f_k(x,y) & j \neq l \end{cases} \quad (8)$$

3. R is a column vector in length of $(N-1)\times L$. For the $((j-1)\cdot L+k)$th row of the vector, it can be expressed as:

$$R_{(j-1)\cdot k} = a_{jk} \quad (9)$$

After calculating the stitching coefficients with Eqs. (3)–(9), the alignment errors of each subaperture can be removed and the full aperture surface can be obtained. However, the accuracy of relative positions between subapertures is usually limited by the mechanical precision. So the alignment accuracy between subapertures may not meet the stitching requirements. To achieve better stitching accuracy, the two-dimensional cross-correlation calculation is introduced in the stitching algorithm.

Theoretically, the phase data should be consistent at the overlapping areas between every two adjacent subapertures. So it can justify the alignment accuracy between neighboring subapertures in order to meet the stitching requirement.

If it meets the requirement, the full map is obtained after removing the effects of adjustment errors. If not, the relative position relationship between adjacent subapertures can be described as:

$$\begin{cases} x_1 = x_2 + dx + \Delta x \\ y_1 = y_2 + dy + \Delta y \end{cases} \quad (10)$$

where (x_1, y_1) and (x_2, y_2) are the pixel coordinates of two neighboring subapertures respectively, (dx, dy) is the relative coordinate relationship between these two subapertures, and it is obtained by mechanical reading. $(\Delta x, \Delta y)$ is the accurate position relationship between the above two subapertures which is to be calculated.

$(\Delta x, \Delta y)$ can be calculated with the two-dimensional cross-correlation algorithm using the phase data from adjacent subapertures as $F ** G$ where the position of the peak in the calculation is $(\Delta x, \Delta y)$.

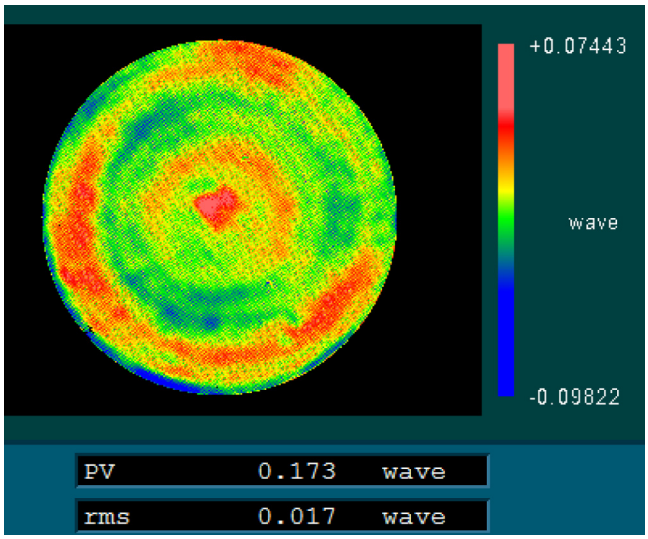

Fig. 4. Full aperture surface of hyperboloid mirror.

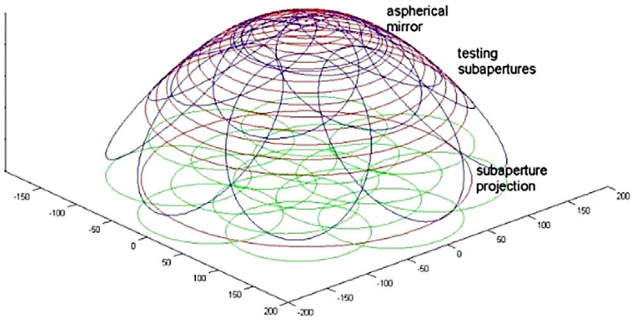

Fig. 5. Subapertures arrangement.

3. Simulation

To prove the concept, we simulate the proposed non-null stitching method to the convex aspheric surface characterization. For a convex hyperboloid surface whose conic constant k is −1.8 in 4000 mm radius of curvature and 300 mm diameter, the original surface in full aperture is shown in Fig. 4.

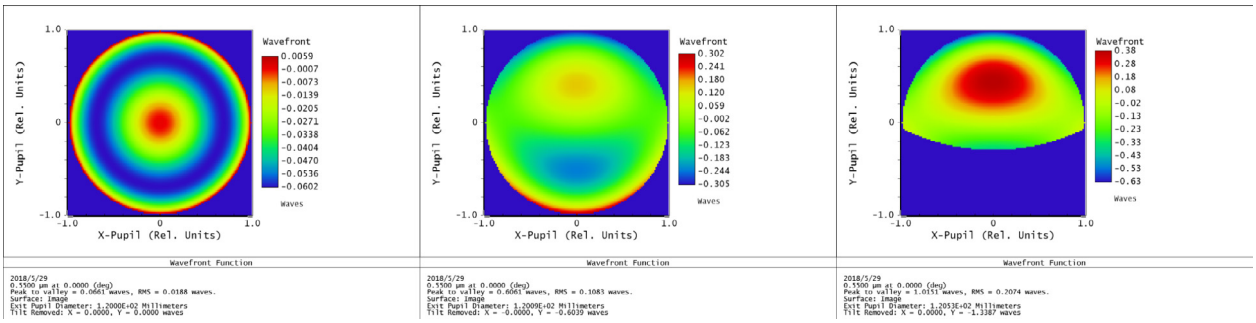

(a) (b) (c)

Fig. 6. Retrace errors of subapertures. (a) retrace error for central subaperture (b) retrace error for the off-axis subaperture in the first ring $d = 60$ mm (c) retrace error for the off-axis subaperture in the second ring $d = 130$ mm.

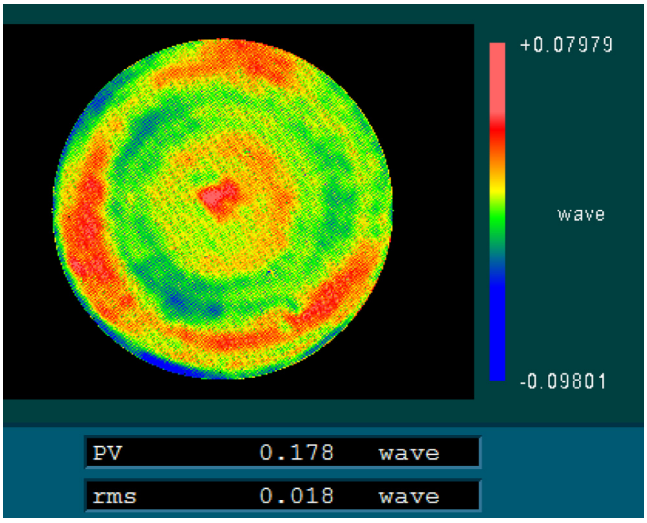

Fig. 7. Stitching map.

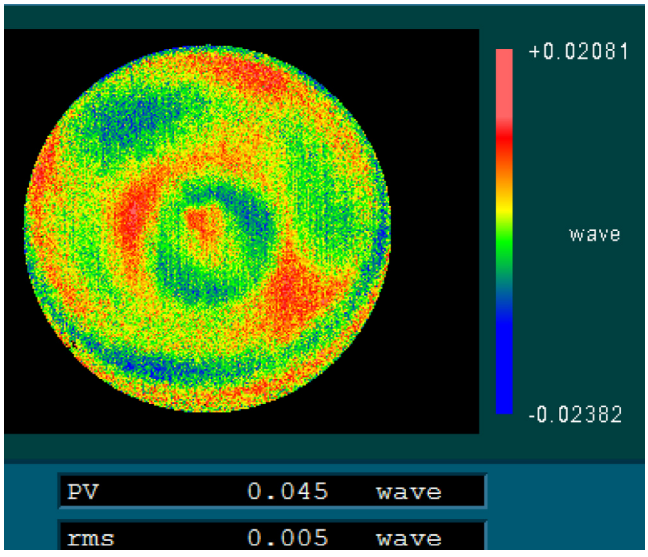

Fig. 8. Residual map.

The convex full aperture is covered by fifteen subapertures, including a central subaperture and 14 off-axis subapertures consist of two rings, as shown in Fig. 5.

In the testing, a 150 mm interferometer with an F#30 standard transmission sphere is chosen to test each subaperture. For the central subaperture and two rings of off-axis subapertures in the testing, the performances of the retrace error are shown in Fig. 6 (a–c) respectively.

By adding the alignment errors such as tip/tilt to each subaperture and considering the 2 μm alignment accuracy along X, Y and Z directions, the non-null stitching algorithm yields the full-aperture map as shown in Fig. 7. In the simulation, the stopping criterion of the stitching is that the RMS of the residual map between every two adjacent subapertures is less than 3 nm. After 3 circles of iteration, the relative stitching is accomplished. In order to evaluate the performance of the non-null stitching algorithm, the residual map is calculated by subtracting the data between the stitching map and the original full aperture map point by point, as shown in Fig. 8.

It can be seen from Figs. 4 and 7 that the stitching map is in consistent with the original full aperture map. The PV and RMS of the residual map between them (Fig. 8) is 0.045λ and 0.005λ ($\lambda = 632.8$ nm) respectively which means that the stitching can be accomplished with our proposed non-null subaperture stitching method very well.

4. Experimental verification

In the experiment, the effective aperture of the convex hyperboloid mirror is 260 mm while the aperture is 300 mm. The conic constant k is −2.2 and the vertex radius of the convex mirror is about 4100 mm. A 5-dof platform and a 150 mm interferometer with an F#30 standard transmission sphere are applied for the stitching testing as shown in Fig. 9. 5-dof platform include the X, Y, Z, A and C axis. The range of movement and relative accuracy of each axis can be found in Table 1. Considering the parameters of test mirror and standard transmission sphere used in the experiment, the approximate aperture of the subapertures can be calculated with Eq. (11). According to the size relationship between subapertures and full-aperture, nine subapertures are designed to cover the effective aperture of the mirror as shown in Fig. 10 and the measured subapertures are shown in Fig. 11.

Table 1
Description of 5-dof platform.

Axis	Range of movement	accuracy
X	1000 mm	0.01 mm
Y	500 mm	0.01 mm
Z	800 mm	0.02 mm
A	90°	4″
C	360°	10″

$$D_{\text{sub}} \approx \frac{R}{F^{\#}} = \frac{4100}{30} \approx 137 \text{ mm} \tag{11}$$

In the testing, for the central subaperture, the retrace error behaves like a combination of power and spherical aberrations which is added

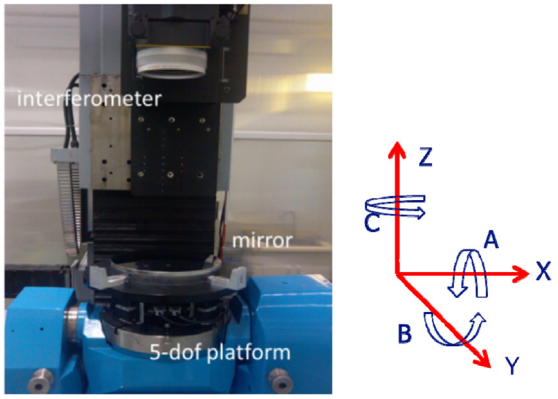

Fig. 9. Experimental setup.

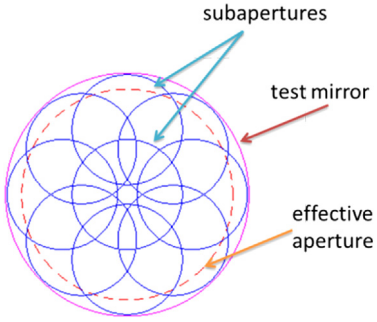

Fig. 10. Subapertures arrangement.

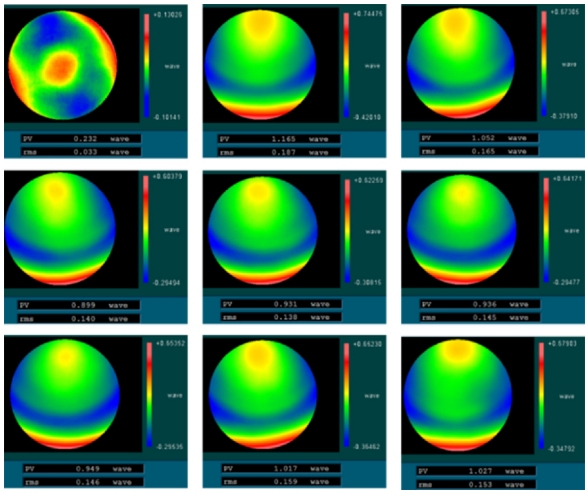

Fig. 11. Measured subapertures.

to the testing map as shown in Fig. 12. For the off-axis subaperture, the behavior of the retrace error is shown in Fig. 13.

After removing the retrace error and retrace coordinate error from each subaperture testing map, the full aperture stitching map can be achieved according to the algorithm described in Section 2.2, as shown in Fig. 14. In the experiment, the stopping criterion of the stitching is that the RMS of the residual map between every two adjacent subapertures is less than 5 nm. After 6 circles of iteration, the relative stitching is accomplished.

Usually the stitching accuracy can be evaluated by comparing the stitching result with the full aperture testing result. However, it is

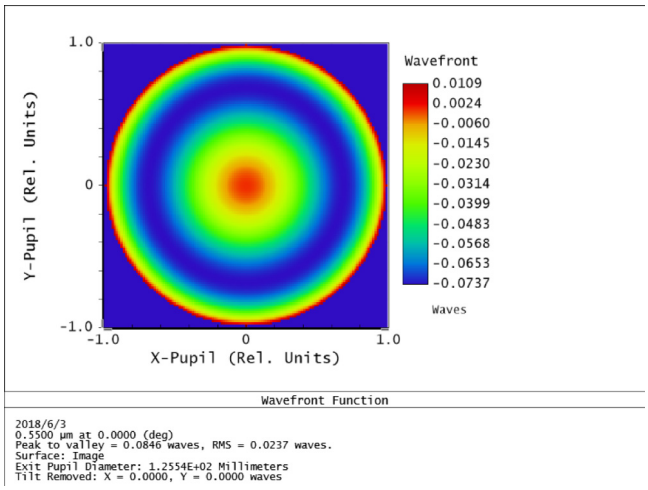

Fig. 12. Retrace error for rotational symmetric subaperture.

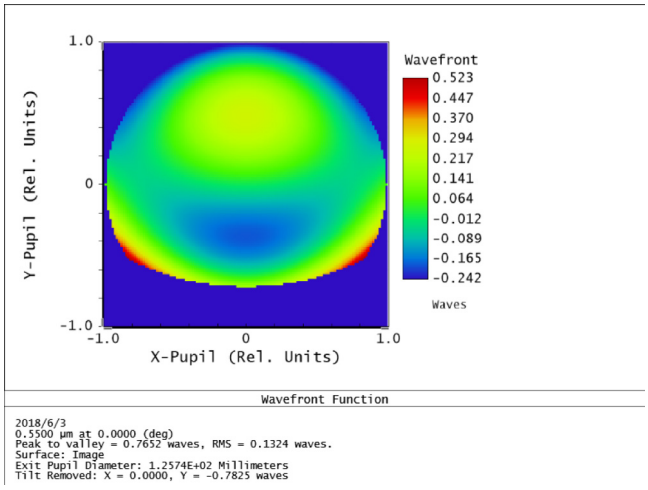

Fig. 13. Retrace error for off-axis subapertures.

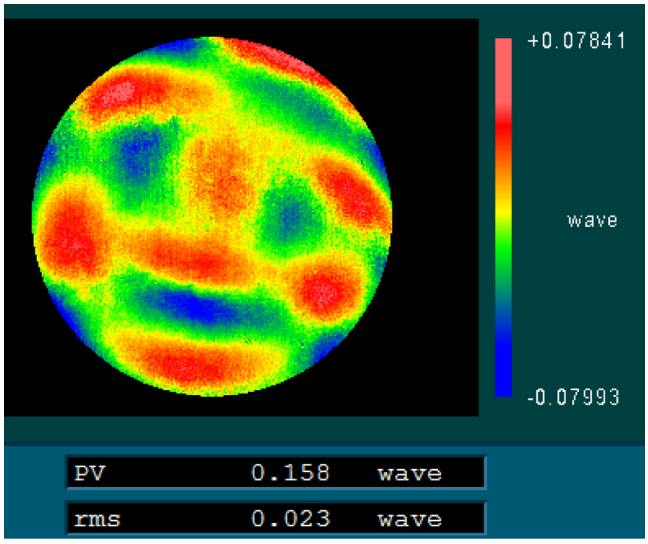

Fig. 14. Stitching map.

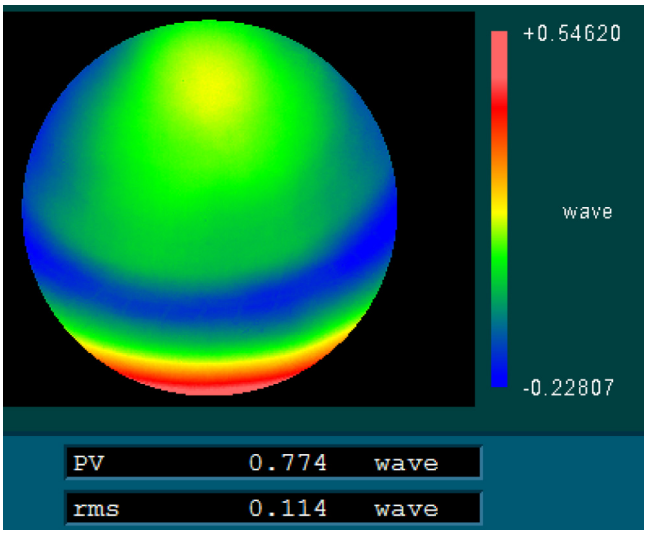

Fig. 15. Self-examine subaperture.

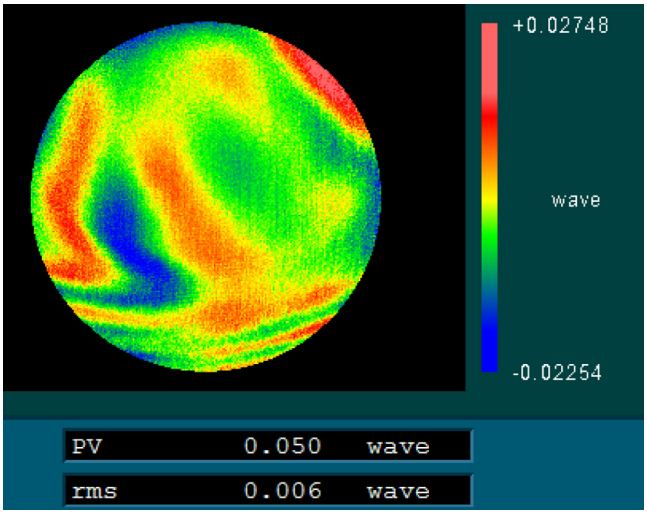

Fig. 16. Residual map.

difficult to get the full map simultaneously for flat or convex mirrors with large apertures. In this case, to evaluate the stitching accuracy, another set of subaperture different from the ones used for stitching is chosen for self-examination, as shown in Fig. 15. The residual map is calculated by subtracting the data between the stitching result and the self-examine subaperture result, as shown in Fig. 16.

It is shown that there is no low order aberration in the residual map and the PV and RMS errors of the residual map are 0.05 λ and 0.006 λ respectively (λ = 632.8 nm). Considering the alignment accuracy in X and Y direction in the testing and the environmental effect, the residual is acceptable and the non-null stitching is feasible in the aspheric surface stitching testing.

5. Conclusion

A non-null stitching testing method is proposed to measure convex aspheric surfaces in a non-null configuration. The retrace error in the non-null aspheric testing is analyzed based on the ray tracing method. A stitching algorithm based on the two-dimensional cross-correlation algorithm and the least square method for non-null stitching testing is developed. Computer simulation results show that the non-null stitching testing is feasible in testing convex aspheric surfaces. To further justify our stitching model, we have tested a convex hyperboloid surface in a comparison experiment. So far the experimental study is only for mild aspheric surfaces. It is expected that the proposed method can also test strong convex aspheric surfaces and freeform surfaces.

References

[1] D. Malacara, Optical Shop Testing, Wiley, 2007.
[2] S. Tomoyoshi, M. Michal, N. Yuki, et al., Color computer-generated hologram generation using the random phase-free method and color space conversion, Appl. Opt 55 (15) (2016) 4159–4165.
[3] Jing Wang, Yunlong Sheng, Design quadrilateral apertures in binary computer-generated holograms of large space bandwidth product, Appl. Opt 55 (27) (2016) 7636–7644.
[4] R. Alata, G. Pariani, F. Zamkotsian, et al., Programmable CGH on photochromic plates coded with DMD generated masks, Opt. Express 25 (6) (2017) 6945–6953.
[5] M.W. Richard, L.W. Gavin, J.C. Joshua, et al., High-contrast pattern reconstructions using a phase-seedd point CGH method, Appl. Opt 55 (7) (2016) 1703–1712.
[6] Han Gu Kim, Yong Man Ro, Ultrafast layer based computer-generated hologram calculation with sparse template holographic fringe pattern for 3-D object, Opt. Express 25 (24) (2016) 30418–30427.
[7] M. Deniz, U. Erdem, U. Hakan, Non-iterative phase hologram computation for low speckle holographic image projection, Opt. Express 24 (5) (2016) 4462–4476.
[8] C.J. Kim, J.C. Wyant, Subaperture test of a large flat or a fast aspheric surface, J. Opt. Soc. Amer. 71 (1981) 1587.
[9] X. Hou, F. Wu, L. Yang, et al., Experimental study on measurement of aspheric surface shape with complementary annular subaperture interferometric method, Opt. Express 15 (20) (2007) 12890–12899.
[10] H.Y. Xu, H. Xian, Y.D. Zhang, Comparison of two stitching algorithms for annular subaperture hartmann shack testing method, Proc. SPIE 7849 (2010) 78491Q-1–78491Q-7.
[11] Y.F. Wen, H.B. Cheng, Hon-Yuen Tam, et al., Modified stitching algorithm for annular subaperture stitching interferometry for aspheric surfaces, Appl. Opt. 52 (23) (2013) 5686–5694.
[12] Yongfu Wen, Haobo Cheng, Further investigations of stitching model for annular subaperture interferometric testing based on Zernike annular polynomials, Optik 126 (2015) 2236–2241.
[13] Lei Zhang, Dong Liu, Yu Liu, Jingxiao Liu, Jingsong Li, Benli Yu, Validation of simultaneous reverse optimization reconstruction algorithm in a practical circular subaperture stitching interferometer, Opt. Commun. 403 (2017) 41–49.
[14] M. Otsubo, K. Okada, J. Tsujiuchi, Measurement of large plane surface shapes by connecting small-aperture interferograms, Opt. Eng. 33 (1994) 608–613.
[15] Dong Liu, Yongying Yang, Chao Tian, Yongjie Luo, Lin Wang, Practical methods for retrace error correction in nonnull aspheric testing, Opt. Express 17 (9) (2009) 7025–7035.
[16] Tu Shi, Dong Liu, Yuhao Zhou, Tianliang Yan, Yongying Yang, Lei Zhang, Jian Bai, Yibing Shen, Liang Miao, Wei Huang, Practical retrace error correction in non-null aspheric testing: a comparison, Opt. Commun. 383 (2017) 378–385.
[17] P. Su, J.H. Burge, R.E. Parks, Application of maximum likelihood reconstruction of subaperture data for measurement of large flat mirrors, Appl. Opt. 49 (2010) 21–31.
[18] Zixin Zhao, Hong Zhao, Feifei Gu, Hubing Du, Kaixing Li, Non-null testing for aspheric surfaces using elliptical sub-aperture stitching technique, Opt. Express 22 (5) (2014) 5512–5520.
[19] Lisong Yan, Xiaokun Wang, Ligong Zheng, Xuefeng Zeng, Haixiang Hu, Xuejun Zhang, Experimental study on subaperture testing with iterative triangulation algorithm, Opt. Express 21 (19) (2013) 22628–22644.
[20] S.Y. Chen, S.Y. Li, Y.F. Dai, et al., Experimental study on subaperture testing with iterative stitching algorithm, Opt. Express 16 (7) (2008) 4760–4765.
[21] Shanyong Chen, Shuai Xue, Yifan Dai, Shengyi Li, Subaperture stitching test of large steep convex spheres, Opt. Express 23 (22) (2015) 29047–29058.